ceramics

MDPI

Article

Thermally Activated $Al(OH)_3$: Part I—Morphology and Porosity Evaluation

Bogdan Stefan Vasile [1,2,*], Gheorghe Dobra [3], Sorin Iliev [4], Lucian Cotet [4], Ionela Andreea Neacsu [1,2], Adrian Ionut Nicoara [1,2], Vasile Adrian Surdu [1,2], Alina Boiangiu [4] and Laurențiu Filipescu [1]

1 Faculty of Applied Chemistry and Materials Science, University Politehnica of Bucharest, 060042 Bucharest, Romania; neacsu.a.ionela@gmail.com (I.A.N.); adi.nicoara18@gmail.com (A.I.N.); adrian.surdu@upb.ro (V.A.S.); laurentiu_filipescu@yahoo.co.uk (L.F.)
2 National Research Center for Micro and Nanomaterials, University Politehnica of Bucharest, 060042 Bucharest, Romania
3 Alro Slatina SA, Pitesti Street, No. 116, 230048 Slatina, Romania; dobra@alro.ro
4 Alum Tulcea SA, Isaccei Street, No. 82, 820228 Tulcea, Romania; siliev@alum.ro (S.I.); lcotet@alum.ro (L.C.); aboiangiu@alum.ro (A.B.)
* Correspondence: bogdan.vasile@upb.ro

Abstract: Aluminum hydroxide is an essential material for the industrial production of ceramics (especially insulators and refractories), desiccants, absorbents, flame retardants, filers for plastics and rubbers, catalysts, and various construction materials. The calcination process of $Al(OH)_3$ first induces dehydration and, finally, results in α-Al_2O_3 formation. Nevertheless, this process contains various intermediary steps and has been proven to be complicated due to the development of numerous transitional alumina. Each step of the investigation is vital for the entire process because the final properties of materials based on aluminum trihydroxide are determined by their phase composition, morphology, porosity, etc. In this paper, five dried, milled, and size-classified aluminum hydroxide specimens were thermally treated at 260, 300, and 400 °C; then, they were studied in order to identify the effects of temperature on their properties, such as particle morphology, specific surface area, pore size, and pore distribution. The major oxide compounds identified in all samples were characteristic of bauxite—namely, Al_2O_3 * $3H_2O$, SiO_2, Fe_2O_3, Na_2O, and CaO. Particles with smaller sizes (<10 µm = 76.28%) presented the highest humidity content (~5 wt.%), while all samples registered a mass loss of ~25 wt.% on ignition at 400 °C. The identified particles had the shapes of hexagonal or quasi-hexagonal platelets and resulted in large spherulitic concretions. The obtained results suggest that ceramic powders calcined at 400 °C should be used for applications as adsorbents or catalysts due to their high specific area of about 200–240 m^2/g and their small pore width (3–3.5 nm).

Keywords: alumina; gibbsite; thermal treatment; morphology; absorbent

Citation: Vasile, B.S.; Dobra, G.; Iliev, S.; Cotet, L.; Neacsu, I.A.; Nicoara, A.I.; Surdu, V.A.; Boiangiu, A.; Filipescu, L. Thermally Activated $Al(OH)_3$: Part I—Morphology and Porosity Evaluation. *Ceramics* **2021**, *4*, 265–277. https://doi.org/10.3390/ceramics4020021

Academic Editors: Ashutosh Goel and Gilbert Fantozzi

Received: 14 April 2021
Accepted: 28 May 2021
Published: 3 June 2021

1. Introduction

Al_2O_3 is industrially manufactured at Alum SA Tulcea from bauxite (Sierra Leone), a sedimentary rock consisting mostly of aluminum and iron minerals—such as gibbsite ($Al(OH)_3$), aluminous goethite ($(Fe_{1-x}Al_x)O(OH)$), aluminous hematite ($(Fe_{1-x}Al_x)_2O$), ilmenite ($FeTiO_3$), kaolinite ($Al_4(OH)_8(Si_4O_{10})$), quartz (SiO_2), and other minor minerals—in both crystalline and amorphous forms through the Bayer process [1]. This process is based on the reaction between ground bauxite and a sodium aluminate solution (molar ratio of Na_2O/Al_2O_3: 1.75 to 1.85), which usually takes place under pressure and in temperatures of 140–150 °C. After the Bayer digestion stage and the removal of the iron and silica compounds (sodalite and cancrinite) and other impurities, the aluminum hydroxide is precipitated from the concentrated aluminate solutions by seeding and cooling to 50–55 °C and is then filtrated and washed on a pan filter. A small portion of the raw wet aluminum

hydroxide is sent to a newly built line for the production of special grades of dried, milled, and classified aluminum hydroxide. These new grades of classified aluminum hydroxide are used to obtain activated alumina powders with specific thermal treatments. Alumina are also obtained from other precursors (chlorides, sulfates, dawsonites, etc.) through calcination at temperatures higher than 300 °C. It was observed that the phases obtained and their final morphologies and surface properties highly depended on their properties of their precursors [2]. Hence, the $AlCl_3$ precursor generated boehmite, while the use of $Al(NO_3)_3 \cdot 9H_2O$ led to bayerite [3]. Corundum (α-Al_2O_3) is the most stable form of Al_2O_3 and can be obtained if a high enough temperature is used [4–6].

During the calcination process, gibbsite undergoes successive stages of dehydration and dehydroxylation until the final crystalline phase, α-Al_2O_3, is obtained. There are some known transition pathways, each of them including several transitional and stable alumina phases. Some of these phases exhibit remarkable properties, facilitating their use as precursors or even final products in applications such as desiccants, absorbents, flame retardants, filers for plastics and rubbers, catalysts, and various construction materials [7,8]. However, various intermediary transitions can be completely missed or concluded halfway by the activation factors, such as the heating rate, impurity nucleation control, and preliminary mechanical gibbsite activation. At any temperature at which the calcination ends, the product is a mixture of a few crystalline phases and variable quantities of amorphous alumina [9,10]. For example, boehmite forms γ-Al_2O_3 when calcined at 300–500 °C, δ-Al_2O_3 when treated at higher temperatures (700–800 °C), or θ-Al_2O_3 at 900–1000 °C before transforming into the final phase: α-Al_2O_3 [11].

The effect of grinding activation on the dried and precipitated aluminum hydroxide was recently evaluated, and the results showed a strong correlation between the mechanochemical treatment and the formation of a new gibbsite phase on the particles' surface with penta-coordinated Al atoms in its crystalline lattice. This phase is presented as an amorphous, gel-like phase that covers the activated particles as a result of the rapid absorption of water into the fractured surfaces [12]. Several studies have pointed out that the transformation of gibbsite first goes towards a less crystalline phase—partially converted gibbsite—and then towards boehmite, depending on the initial surface area, particle size, and morphology of the particles [13,14]. This distinct transition was first reported by Brown et al., who demonstrated that these transitions are pseudo-morphic and topotactic with respect to the axes of gibbsite. Both partial alumina and boehmite generate so-called transition alumina; at temperatures above 1100 °C, in the end, they lead to corundum [15]. Therefore, the great importance of the thermal properties of gibbsite comes from the fact that gibbsite is the only crystalline form that is able to produce all transition alumina through thermal treatments [6].

In terms of size and morphology, studies in the literature have presented natural or synthetic crystals of gibbsite that are of micrometric size and have morphologies that vary from tabular morphologies with pseudo-hexagonal profiles to prisms with hexagonal bases [16–18]. As for micro- or nano-scaled boehmite, numerous morphologies have been described depending on the dimensionality [8]. Hence, for materials that have crystals that are shaped in two external dimensions (x and y) on the nanometric scale with a third dimension that is significantly bigger (1D), the most commonly encountered morphologies of boehmite are tubes, fibers, whiskers, needles, and rods. For two-dimensional (2D) boehmite materials, lamellar and platelet-shaped morphologies are the most known. Three-dimensional materials are considered to be the most complex and spectacular in terms of morphology; they comprise quasi-cubic or quasi-spherical shapes, along with a wide variety of 1D or 2D crystal assemblies, which are often called "urchin-like", "flower-like", "hollow microspheres", etc. [7,19].

Because gibbsite and boehmite are mostly produced through the calcination of aluminum hydroxide, their specific features, such as their dimensions and morphology, are closely connected to those of the initial $Al(OH)_3$ [20].

The process of manufacturing aluminum hydroxide of advanced purity for use as a future raw material for the production of special alumina started with the investigation of the purity of available raw materials [21]. The purpose of this work is to continue to improve the industrial process of the synthesis of special alumina from $Al(OH)_3$ by investigating the changes in morphology, porosity, and specific surface area of several thermally treated aluminum hydroxide ceramic powders. The calcination temperatures (260, 300, and 400 °C) were intentionally chosen to cause gibbsite amorphization at low temperatures in order to obtain larger specific surface areas and uniform pore distributions in the newly formed crystalline and amorphous phases. According to the literature, the effects expected at 260 °C come from the partial transition of gibbsite to boehmite and the associated metastable and amorphous phases. The next temperature, 300 °C, is placed right at the end of the gibbsite-to-boehmite transition, while at 400 °C, the boehmite might be partially converted into metastable and amorphous γ-alumina phases [22,23].

Hence, the first goal of this research was to investigate how these new materials respond to mild thermal activation and if their properties (specific surface area, porosity, and particle size distribution) sustain eventual uses as low-temperature semi-calcined alumina.

2. Materials and Methods

2.1. Sample Preparation

Aluminum hydroxide ceramic powders were collected from the industrial-size unit recently opened at SC ALUM SA, as recently described by Dobra et al. [21]. This unit was designed to produce several different grades of dried and milled aluminum hydroxide with specific particle size distributions. Additional information regarding the initial four representative specimens of milled aluminum hydroxide is presented in Table 1. The powders were first dried at 60 °C for 24 h, then calcined at 260, 300, and 400 °C for 2 h, with a heating rate of 5 °C/min. The samples were slowly cooled in the oven until they reached room temperature and were then weighed.

Table 1. Aluminum hydroxide ceramic powders.

Sample Name	Details of the Dimension Classes after Milling
GDAH-02	<45 μm = 98.29%
GDAH-03	<20 μm = 92.13%
GDAH-04	<10 μm = 76.28%
GDAH-05	<45 μm = 0.001%; >150 μm = 6.54%

2.2. Characterization Methods

An X-ray sequential fluorescence spectrometer (XRF; Thermo Fisher Scientific ARL PERFORM'X, Waltham, MA, USA) equipped with an X-ray tube with a Rh anode and a Be window of 30 μm was used for qualitative and quantitative analysis of the elements. The entire surface of the sample was analyzed in a dry He flow.

The humidity (wt.%) and weight loss on ignition (LOI; wt.%) were evaluated for each sample and after each thermal treatment using Equations (1) and (2). Hence, the powders were placed in ceramic crucibles and weighed initially, after drying, and after each thermal treatment at temperature *t* (260, 300, and 400 °C).

$$\text{Humidity (wt. \%)} = \frac{(m_i - m_d)}{m_i} \times 100 \quad (1)$$

$$\text{LOI (wt. \%)} = \frac{(m_d - m_t)}{m_d} \times 100 \quad (2)$$

where:

m_i—the initial mass of the sample, before drying (g);
m_d—the mass of the dried sample (g); and

m_t—the mass of the sample when calcined at temperature *t* (g).

A Quanta Inspect F50 FEG scanning electron microscope (Thermo Fisher, Eindhoven, Netherland), with a resolution of 1.2 nm and an Everhart–Thornley secondary electron detector (ETD), which was equipped with an energy-dispersive X-ray (EDS) analyzer (resolution of 133 eV at MnKα, Thermo Fisher Scientific, Waltham, MA, USA), were used to analyze the morphologies and the chemical compositions of the samples.

The volumetric N_2 adsorption (Brunauer–Emmett–Teller; BET) analysis was performed on a Gemini V2 model 2380 (Micromeritics Instruments Corporation, Norcross, GA, USA) surface area and pore size analyzer in order to determine the specific surface area (SSA) of the powders and the pore volume. The adsorption isotherms were registered by determining the amount of gas adsorbed at various relative pressure values and at a constant temperature (77 K and pressure between 780 and 7.8 mmHg). Conversely, the desorption isotherms were obtained by measuring the gas that was removed as the pressure was reduced.

3. Results and Discussion

The chemical composition of the ceramic powders before calcination in terms of metallic oxides was analyzed with XRF, and the results are presented in Table 2. The compounds identified were characteristic of bauxite, the starting material in the Bayer process. It is known that bauxite contains various forms of aluminum minerals—with hydrargillite (gibbsite; Al_2O_3 $3H_2O$) being the most common form—along with several aluminosilicates, which are usually in the form of kaolinite ($Al_2O_3 \cdot 2SiO_2 \cdot 2H_2O$), hematite ($Fe_2O_3$), etc. [24,25]. The smaller amounts of non-aluminous oxides identified in the samples can be associated with the previously described process of removing impurities through sedimentation and filtration [21,25].

Table 2. Major metallic oxides (wt.%) identified through XRF analysis of the chemical composition of the ceramic powders.

Sample	GDAH-02	GDAH-03	GDAH-04	GDAH-05
Compound	wt.%	wt.%	wt.%	wt.%
Al_2O_3 $3H_2O$	63.90	64.26	64.11	64.24
Na_2O	0.0775	0.0989	0.0885	0.376
SiO_2	0.0619	0.0537	0.0591	0.0881
CaO	0.0408	0.0377	0.0391	0.0546
Fe_2O_3	0.0126	0.0117	0.0117	0.0149

The humidity of the ceramic powders is a significant parameter when discussing the conditions of shipping or storage after synthesis, as well as when the chemical and physical characteristics of the materials are evaluated. Water can be present in a sample as either physical water (which is mechanically held on the surface and will mostly evaporate when drying) or chemically bonded water (water of constitution—for example, the water of crystallization) [26]. Figure 1 presents the results of the humidity evaluation for the aluminum hydroxide samples. It is easily observed that the humidity content was very low for all samples, reaching a maximum of around 0.25 wt.% in the case of the GDAH-04 sample and a minimum of less than 0.05 wt.% in the case of the GDAH-05 sample. The results can be directly correlated with their corresponding dimension class details, which were previously presented in Table 1. Particles of smaller sizes (<10 μm = 76.28%) have a higher adsorption capacity due to their increased surface area; therefore, larger numbers of water molecules become attached, which results in a high humidity content. On the contrary, most particles from the GDAH-05 sample had dimensions that varied in the range of 45–150 μm, which was associated with a smaller surface energy and lower ability to attract water molecules, resulting in a low humidity content.

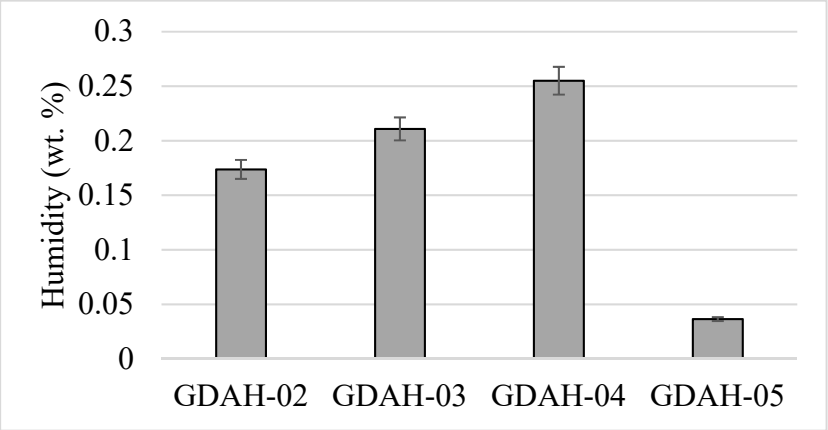

Figure 1. Humidity evaluation for the samples dried at 60 °C for 24 h.

Apart from water, ceramic materials usually have additional volatile components that are eliminated through calcination at higher temperatures. Examples of thermally unstable components that are present in inorganic powders are carbonates, nitrates, and sulfates, which decompose at high temperatures, or other salts, which may also oxidize or reduce [27]. Carbon can also be present, but it is eliminated after oxidation. It is very important to determine the content of these volatile components in order to properly predict their final mass and physical properties, especially when designing ceramic materials.

For this analysis, the samples were thermally treated at high temperatures; therefore, all of the remaining physical water was first eliminated, followed by the elimination of the chemically bonded water. In Figure 2, the results of weight loss on ignition for the samples calcined at 260, 300, or 400 °C for 2 h are graphically represented. All samples suffered a mass loss of less than 5 wt.% when calcined at 260 °C, which could be associated with the water that resulted from a partial dehydroxylation of $Al(OH)_3$; this phenomenon is usually reported in the literature to occur between 210 and 260 °C.

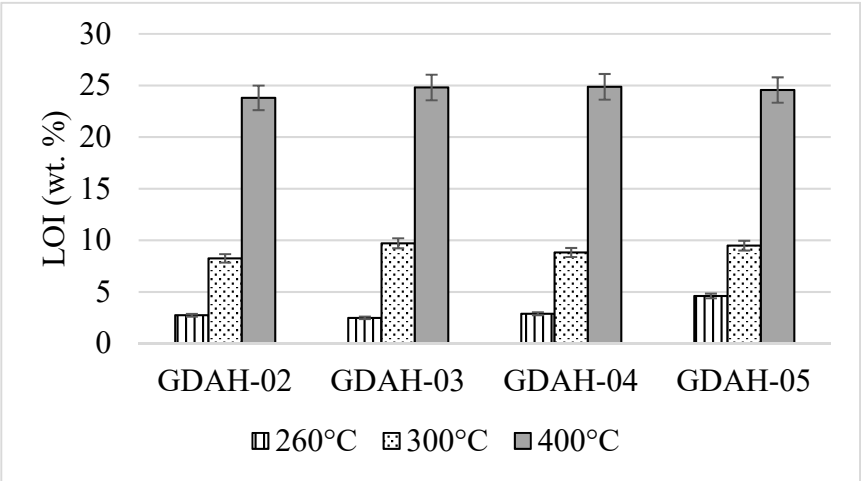

Figure 2. Weight loss on ignition results for the samples calcined at 260, 300, or 400 °C for 2 h.

The $Al(OH)_3$ decomposition continued with the increase in temperature. Hence, for the samples calcined at 300 °C, the LOI was around 10%, with no significant differences between powders; this corresponded to the additional loss of water due to the dehydroxylation. A significant difference from the previous results was registered for all of the samples when calcined at 400 °C. In this case, the LOI (wt.%) was ~25%, and it can be assumed that the transformation into AlO(OH) (boehmite) or partial alumina was finalized and the volatile compounds were eliminated [28].

Morphological modifications of the thermally treated ceramic powders were investigated by means of SEM analysis, and the resulting images are presented in Figures 3–6.

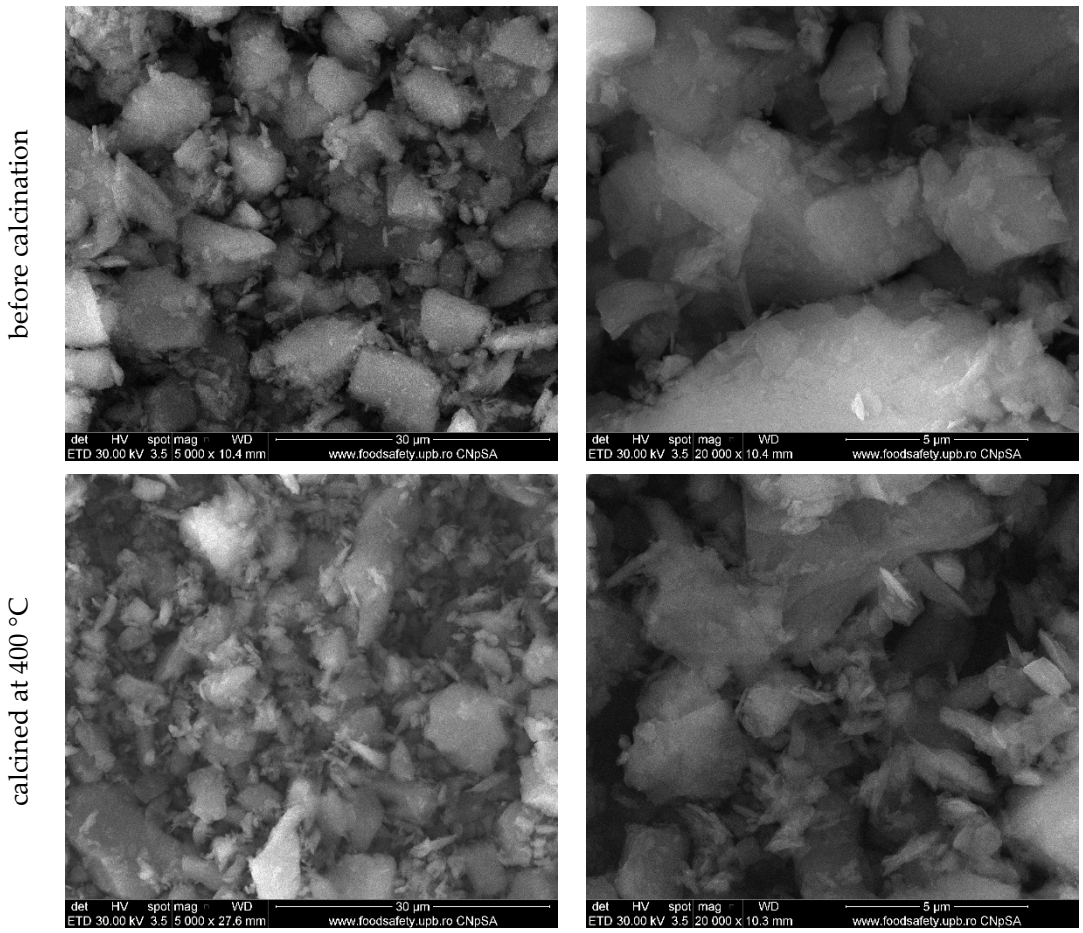

Figure 3. SEM images of the GDAH-02 powder before the thermal treatment and after calcination at 400 °C.

Before the calcination, no significant differences between the particles from the GDAH-02 (Figure 3), GDAH-03 (Figure 4), and GDAH-04 (Figure 5) samples were observed. They all had morphologies that were characteristic of the original Bayer gibbsite—comprised of hexagonal or quasi-hexagonal platelet shapes with asymmetrical lines—as a result of the mechanical grinding step from their fabrication process. These three powders corresponded to the class of small dimensions (a particle size of <45 µm). The SEM images confirmed their micrometric size and their non-homogeneity in terms of their dimensions (small particles were found around larger clusters).

During the thermal treatment, the gibbsite-to-boehmite conversion was triggered, which significantly reduced the particle size, especially for the powders of the small dimension class. The morphology became more elongated and had a greater tendency for agglomeration. This topotactic phase transition of gibbsite to boehmite at low temperatures was most probably started by the volatilization of water from the layered structure of gibbsite [29].

The GDAH-05 sample exhibited a different behavior in terms of its morphology, which was probably due to the larger size of the constituent particles (<45 µm = 0.001%; >150 µm = 6.54%) in comparison with the other ceramic powders (Figure 6). Hence, large spherulitic concretions were observed; they were very well dispersed and homogenous in shape and size, similar to those in the literature [12,30]. Upon closer examination, these agglomerations also proved to have formed from pseudo-hexagonal-platelet-shaped crystals,

suggesting that the other samples were, in fact, small fragments that were mechanically detached from these original, larger concretions.

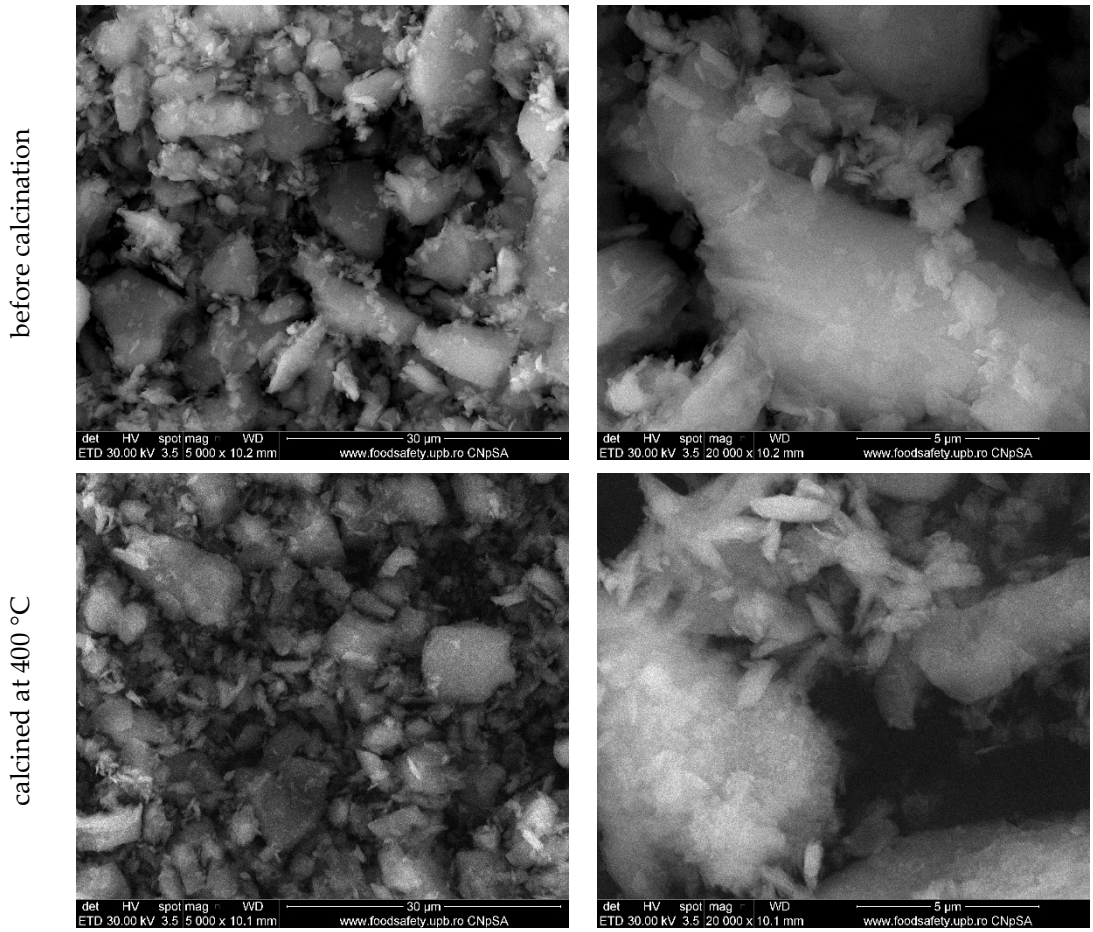

Figure 4. SEM images of the GDAH-03 powder before the thermal treatment and after calcination at 400 °C.

Table 3 presents results of the BET analysis in terms of the specific surface area and the pore width of the ceramic powders before and after each thermal treatment. For all samples, an increase in surface area was observed, and this was associated with a decrease in pore size. This is a common behavior that is likely because a smaller pore width allows a higher number of pores per unit of volume of the material and, hence, generates larger free surfaces.

The BET and Langmuir specific areas of the powders increased smoothly with the increase in temperature up to 300 °C; then, a more rapid increase was observed between 300 and 400 °C. Based on reports from the literature, a specific surface area greater than 125 m^2/g registered after a thermal treatment of $Al(OH)_3$ at a low temperature can be associated with the formation of thermodynamically stable γ-phase alumina [17,31,32].

Figure 7 depicts the nitrogen adsorption−desorption BET isotherms of all of the samples. The results for the samples that were un-calcined or calcined at 260 °C fit the type III adsorption isotherm, which corresponds to nonporous materials. After calcination at a higher temperature, the isotherms shifted towards those corresponding to microporous structures with a higher adsorption capacity. The results were in good correlation with the specific area and average pore width that were previously presented.

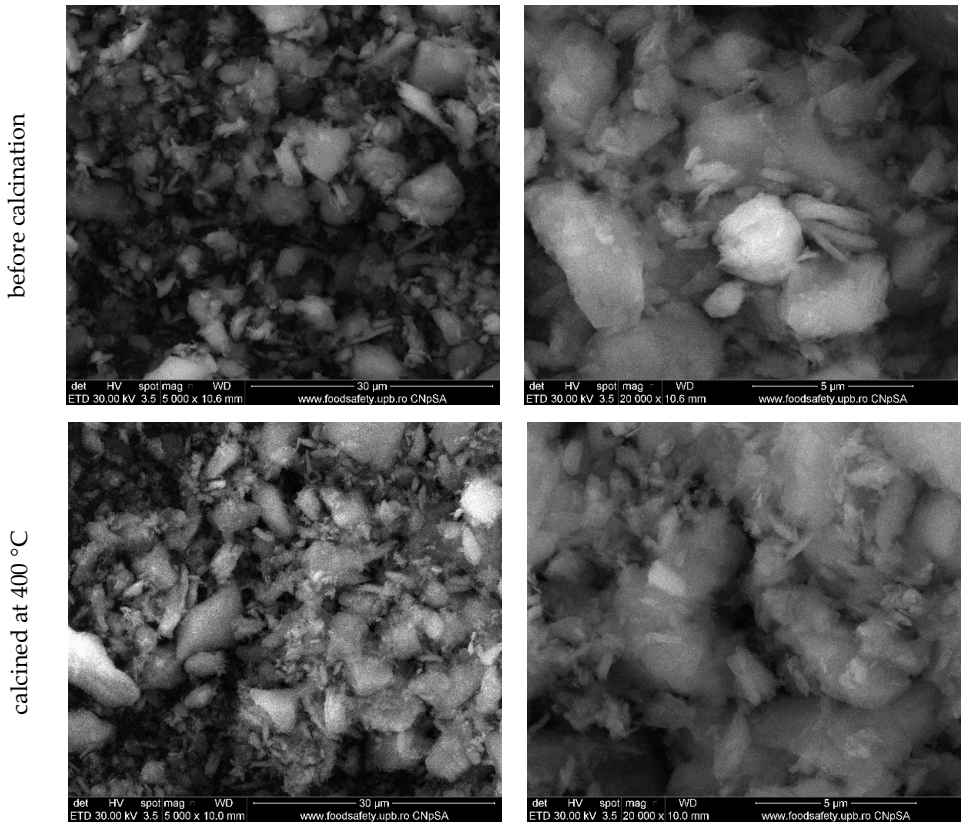

Figure 5. SEM images of the GDAH-04 powder before the thermal treatment and after calcination at 400 °C.

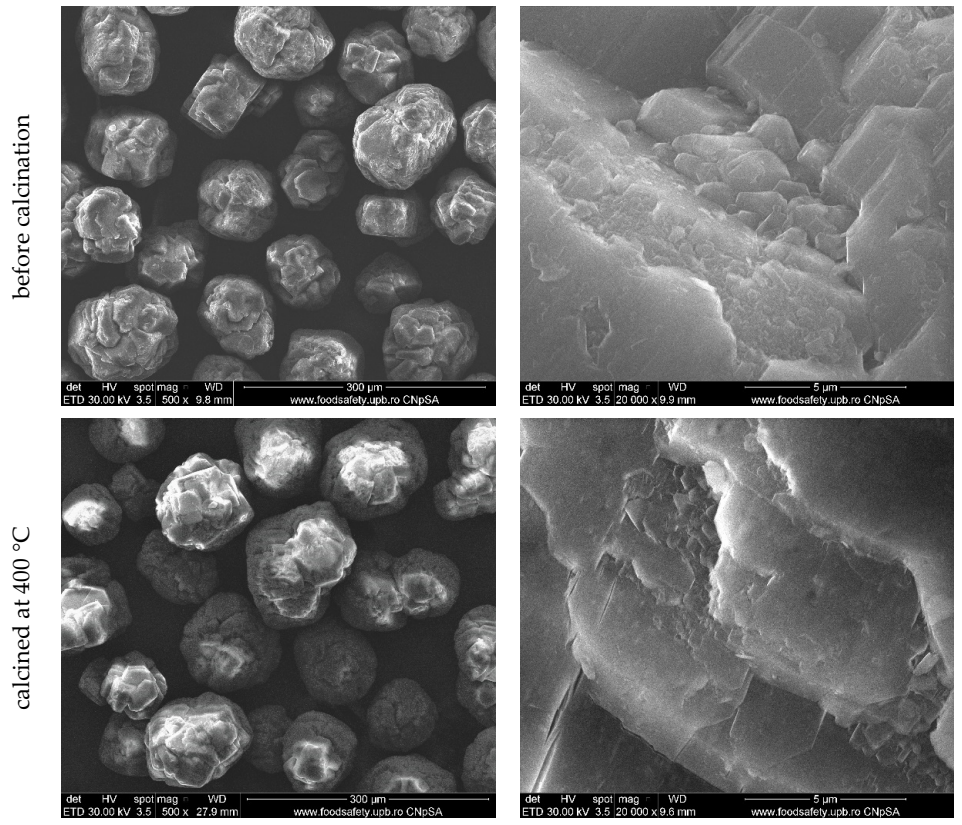

Figure 6. SEM images of the GDAH-05 powder before the thermal treatment and after calcination at 400 °C.

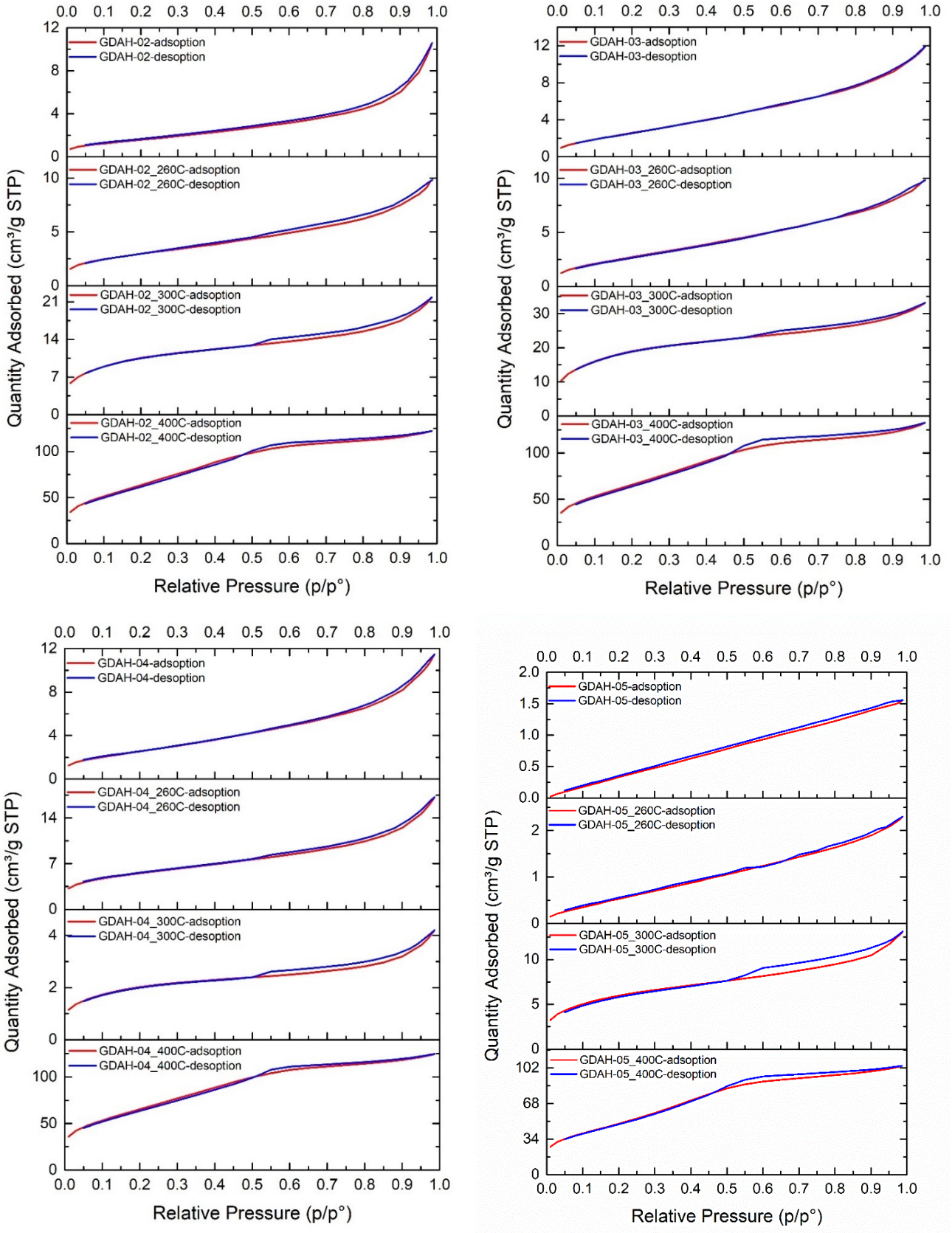

Figure 7. Nitrogen adsorption−desorption BET isotherms of the initial samples and of the samples after the thermal treatment at 260, 300, or 400 °C for 2 h.

Table 3. Specific surface area and pore width measurements for the initial samples and samples after thermal treatments at 260, 300, or 400 °C for 2 h.

Sample	BET Specific Area (m^2/g)	Langmuir Specific Area (m^2/g)	Average Pore Width (nm)
GDAH-02	5.9596	8.9199	10.9876
GDAH-02_260 °C	10.6208	15.5593	5.7378
GDAH-02_300 °C	36.3853	52.7869	3.7164
GDAH-02_400 °C	234.4518	345.6202	3.2249
GDAH-03	10.3375	16.0231	7.1186
GDAH-03_260 °C	10.3094	15.5083	5.9023
GDAH-03_300 °C	65.5179	95.2101	3.1337
GDAH-03_400 °C	241.9623	356.6276	3.3867
GDAH-04	9.4725	14.0771	7.4804
GDAH-04_260 °C	19.4569	28.2606	5.4720
GDAH-04_300 °C	6.9195	10.0146	3.7566
GDAH-04_400 °C	238.6443	350.5961	3.2303
GDAH-05	2.2240	7.3240	4.3304
GDAH-05_260 °C	2.2964	3.7623	6.1816
GDAH-05_300 °C	20.8556	30.3694	3.8894
GDAH-05_400 °C	181.5672	267.8954	3.5443

The graphical representation in Figure 8 confirms the influence of the thermal treatment on the pore size distributions in all samples. The initial pore size distributions were observed to be in the range of 0–120 nm with a broad peak around 20–30 nm, which became narrower when the temperature increased. Moreover, a new, sharp, and very narrow pore size distribution maximum was registered below 10 nm for all of the samples calcined at 400 °C. These results are in accordance with the previously discussed specific surface area values, and they are most probably characteristic of porous γ-alumina.

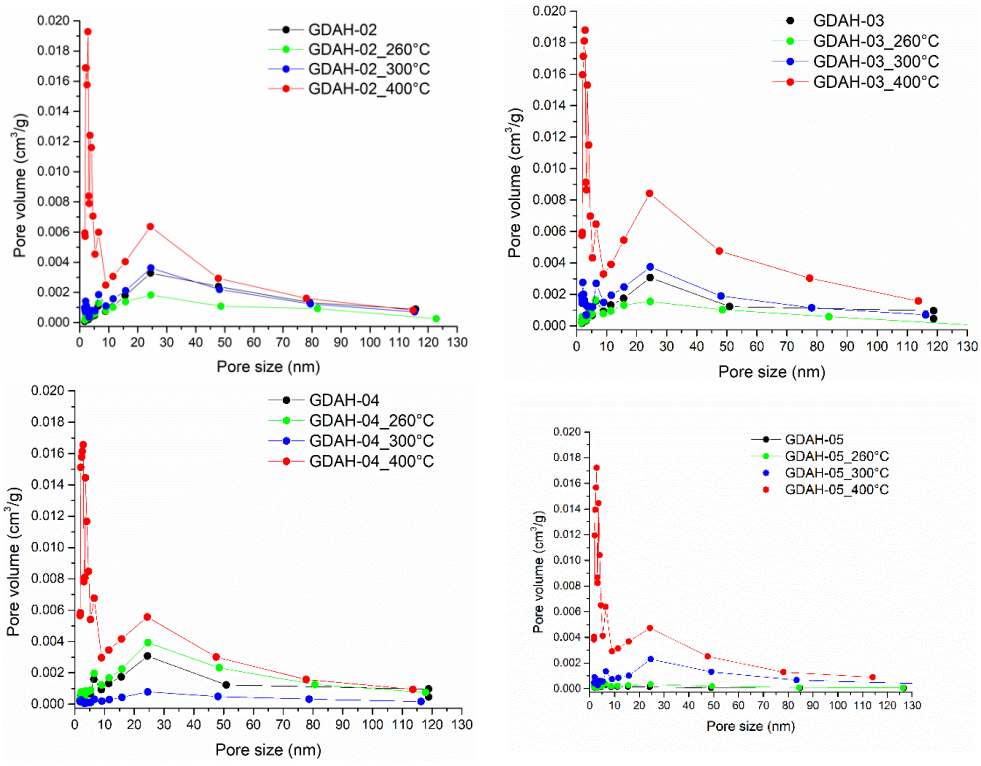

Figure 8. Pore size distribution curves for the initial samples and after thermal treatments at 260, 300, or 400 °C for 2 h.

The results obtained here suggest that ceramic powders calcined at 400 °C have prospective applications in composite adsorbents and catalysts due to their high specific area of about 200–240 m^2/g and their small pore size in comparison with the findings of recent reports [33,34]. For instance, adding small amounts of SiO_2 to γ-Al_2O_3 proved to be good for stabilization, and the resulting porous silica-doped alumina can be a supportive catalyst with improved thermal stability [35].

4. Conclusions

Aluminum hydroxide ceramic powders that were calcined at 260, 300, and 400 °C were evaluated in terms of their chemical composition, morphology, specific surface area, and pore size in order to identify possible effects of variations in the temperature of the thermal treatment. The experimental data were in good agreement with data from the literature and fully justify the events anticipated in the introduction section. Thus, the particle size distribution and the specific surface area are dependent on the temperature and the initial particle size dimensions. A rapid increase in the specific surface area of up to 200–240 m^2/g was observed between 300 and 400 °C, along with an enhanced decrease in the pore width (down to 3–3.5 nm). In addition, the pore size distribution and the large increase in the specific surface area of all of the samples suggest that these powders have the excellent properties required for industrial applications. The mechanisms of the phase transitions of aluminum hydroxide in the above samples; the identification of alumina phases in each stage of calcination; and the full characterization of the dried, milled, and size-classified aluminum hydroxide will be described in the second part of this paper.

Author Contributions: Conceptualization, B.S.V. and L.F.; methodology, G.D., S.I. and L.C.; validation, A.B.; formal analysis, A.I.N.; investigation, V.A.S.; writing—original draft preparation, I.A.N.; writing—review and editing, I.A.N., B.S.V. and L.F.; visualization, A.I.N.; supervision, L.F.; project administration, B.S.V.; funding acquisition, L.F. All authors have read and agreed to the published version of the manuscript.

Funding: This research received no external funding.

Institutional Review Board Statement: Not applicable.

Informed Consent Statement: Not applicable.

Acknowledgments: This study was made possible by the implementation of the "Endow the Research and Development Department of SC ALUM SA Tulcea with independent and efficient research facilities to support the economic competitiveness and business development" project, which was co-funded by the European Regional Development Fund through the Competitiveness Operational Program of 2014–2020. Under this project, the following were purchased and commissioned: "Independent equipment/installation for research and development of the technology for wet aluminum hydroxide classification", "Independent equipment/installation for research and development of technology for obtaining the dried aluminum hydroxide", and "Independent equipment/installation for research and development of the technology for grinding and screening the dried aluminum hydroxide".

Conflicts of Interest: The authors declare no conflict of interest. The funders had no role in the design of the study; in the collection, analyses, or interpretation of data; in the writing of the manuscript; or in the decision to publish the results.

References

1. Padilla, I.; López-Andrés, S.; López-Delgado, A. Effects of Different Raw Materials in the Synthesis of Boehmite and γ- and α-Alumina. *J. Chem.* **2016**, *2016*, 5353490. [CrossRef]
2. Žumbar, T.; Ristic, A.; Dražić, G.; Lazarova, H.; Volvašek, J.; Pintar, A.; Logar, N.Z.; Tusar, N.N. Influence of alumina precursor properties on cu-fe alumina supported catalysts for total toluene oxidation as a model volatile organic air pollutant. *Catalysts* **2021**, *11*, 252. [CrossRef]
3. Osman, A.I.; Abu-Dahrieh, J.K.; Rooney, D.W.; Halawy, S.A.; Mohamed, M.A.; Abdelkader, A. Effect of precursor on the performance of alumina for the dehydration of methanol to dimethyl ether. *Appl. Catal. B Environ.* **2012**, *127*, 307–315. [CrossRef]

4. Shirai, T.; Watanabe, H.; Fuji, M.; Takahashi, M. Structural Properties and Surface Characteristics on Aluminum Oxide Powders. *Annu. Rep. Ceram. Res. Lab. Nagoya Inst. Technol.* **2010**, *9*, 23–31.
5. Pyzalski, M.; Wojcik, M. The dehydroxylation of aluminium hydroxides and the kinetics of α-Al2O3 formation. *J. Therm. Anal.* **1990**, *36*, 2147–2151. [CrossRef]
6. Said, S.; Mikhail, S.; Riad, M. Recent processes for the production of alumina nano-particles. *Mater. Sci. Energy Technol.* **2020**, *3*, 344–363. [CrossRef]
7. Abdelkader, A.; Hussien, B.M.; Fawzy, E.M.; Ibrahim, A.A. Boehmite nanopowder recovered from aluminum cans waste as a potential adsorbent for the treatment of oilfield produced water. *Appl. Petrochem. Res.* **2021**, *1*, 3.
8. Mohammadi, M.; Khodamorady, M.; Tahmasbi, B.; Bahrami, K.; Ghorbani-Choghamarani, A. Boehmite nanoparticles as versatile support for organic–inorganic hybrid materials: Synthesis, functionalization, and applications in eco-friendly catalysis. *J. Ind. Eng. Chem.* **2021**, *97*, 1–78. [CrossRef]
9. Ptacek, P. Processes during Thermal Treatment. In *Strontium Aluminate-Cement Fundamentals, Manufacturing, Hydration, Setting Behaviour and Applications*, 1st ed.; IntechOpen Limited: London, UK, 2014; pp. 97–128.
10. van Gog, H. First-principles study of dehydration interfaces between diaspore and corundum, gibbsite and boehmite, and boehmite and γ-Al2O3: Energetic stability, interface charge effects, and dehydration defects. *Appl. Surf. Sci.* **2021**, *541*, 148501. [CrossRef]
11. Osman, A.I.; Abu-Dahrieh, J.K.; McLaren, M.; Laffir, F.; Rooney, D.W. Characterisation of Robust Combustion Catalyst from Aluminium Foil Waste. *ChemistrySelect* **2018**, *3*, 1545–1550. [CrossRef]
12. Mercury, J.M.R.; Sucupira, J.R.M.; Rodríguez, M.A.; Cabral, A.A.; de Aza, A.H.; Pena, P. Influence of the milling conditions on the thermal decomposition of Bayer gibbsite. *Powder Technol.* **2020**, *362*, 188–196. [CrossRef]
13. Jiao, W.Q.; Yue, M.B.; Wang, Y.M.; He, M.Y. Synthesis of morphology-controlled mesoporous transition aluminas derived from the decomposition of alumina hydrates. *Microporous Mesoporous Mater.* **2012**, *147*, 167–177. [CrossRef]
14. Zhang, X.; Cui, W.; Hu, J.Z.; Wang, H.-W.; Prange, M.P.; Wan, C.; Jaegers, N.R.; Zong, M.; Zhang, H.; Pearce, C.I.; et al. Transformation of Gibbsite to Boehmite in Caustic Aqueous Solution at Hydrothermal Conditions. *Cryst. Growth Des.* **2019**, *19*, 5557–5567. [CrossRef]
15. Brown, J.F.; Clark, D.; Elliott, W.W. The thermal decomposition of the alumina trihydrate, gibbsite. *J. Chem. Soc.* **1953**, 84–88. [CrossRef]
16. Golafshan, N.; Vorndran, E.; Zaharievski, S.; Brommer, H.; Kadumudi, F.B.; Dolatshahi-Pirouz, A.; Gbureck, U.; van Weeren, R.; Castilho, M.; Malda, J. Tough magnesium phosphate-based 3D-printed implants induce bone regeneration in an equine defect model. *Biomaterials* **2020**, *261*, 120302. [CrossRef] [PubMed]
17. Coelho, A.C.V.; Santos, H.d.; Kiyohara, P.K.; Marcos, K.N.P.; Santos, P.d. Surface area, crystal morphology and characterization of transition alumina powders from a new gibbsite precursor. *Mater. Res.* **2007**, *10*, 183–189. [CrossRef]
18. Sweegers, C.; de Coninck, H.C.; Meekes, H.; van Enckevort, W.J.P.; Hiralal, I.D.K.; Rijkeboer, A. Morphology, evolution and other characteristics of gibbsite crystals grown from pure and impure aqueous sodium aluminate solutions. *J. Cryst. Growth* **2001**, *233*, 567–582. [CrossRef]
19. Filho, R.W.N.D.; Rocha, G.D.; Montes, C.R.; Vieira-Coelho, A.C. Synthesis and characterization of boehmites obtained from gibbsite in presence of different environments. *Mater. Res.* **2016**, *19*, 659–668. [CrossRef]
20. Woo, S.; Park, J.H.; Rhee, C.K.; Lee, J.; Kim, H. Effect of thermal treatment on the aluminum hydroxide nanofibers synthesized by electrolysis of Al plates. *Microelectron. Eng.* **2012**, *89*, 89–91. [CrossRef]
21. Dobra, G.; Garcie-Granda, S.; IIiev, S.; Cotet, L.; Hulka, I.; Negrea, P.; Duteanu, N.; Boiangiu, A.; Laurentiu, F. Aluminum hydroxide impurities occlusions and contamination sources. *Rev. Chim.* **2020**, *70*, 65–76. [CrossRef]
22. Baranyai, V.Z.; Kristály, F.; Szűcs, I. Influence of grain and crystallite size on the gibbsite to boehmite thermal transformation. *Stud. Univ. Babes Bolyai Chem.* **2015**, *60*, 27–44.
23. Alex, T.C.; Kailath, A.J.; Kumar, R. Al-Monohydrate (Boehmite) to Al-Trihydrate (Bayerite/Gibbsite) Transformation During High-Energy Milling. *Metall. Mater. Trans. B Process Metall. Mater. Process. Sci.* **2020**, *51*, 443–451. [CrossRef]
24. Keselj, D.; Lazic, D.; Penavin-skundric, J.; Sladojevic, S.; Vasiljevic, L. Determination of Alumina Oxide in Bauxites by X-Ray Fluorescence Analysis. *Glob. J. Sci. Front. Res. Chem.* **2012**, *12*, 1–6.
25. Dobra, G.; Filipescu, L.; Anghelovici, N.; Alistarh, V.; Iliev, S.; Cotet, L. Bauxite Residue Safety Disposal and Possibilities to Further Utilization. Part 1. Acid Soils Remediation. *J. Sib. Fed. Univ. Chem.* **2017**, *10*, 6–21. [CrossRef]
26. Xiao, C.; Shi, P.; Yan, W.; Chen, L.; Qian, L.; Kim, S.H. Thickness and Structure of Adsorbed Water Layer and Effects on Adhesion and Friction at Nanoasperity Contact. *Colloids Interfaces* **2019**, *3*, 55. [CrossRef]
27. García, A.C.; Latifi, M.; Chaouki, J. Kinetics of calcination of natural carbonate minerals. *Miner. Eng.* **2020**, *150*, 106279. [CrossRef]
28. Redaoui, D.; Sahnoune, F.; Heraiz, M.; Raghdi, A. Mechanism and kinetic parameters of the thermal decomposition of gibbsite Al(OH)3 by thermogravimetric analysis. *Acta Phys. Pol. A* **2017**, *131*, 562–565. [CrossRef]
29. Mitsui, T.; Matsui, T.; Kikuchi, R.; Eguchi, K. Microstructural transformation with heat-treatment of aluminum hydroxide with gibbsite structure. *Bull. Chem. Soc. Jpn.* **2009**, *82*, 618–623. [CrossRef]
30. Santos, P.S.; Santos, H.S.; Toledo, S.P. Standard transition aluminas. Electron microscopy studies. *Mater. Res.* **2000**, *3*, 104–114. [CrossRef]

31. Banerjee, S.; Dubey, S.; Gautam, R.K.; Chattopadhyaya, M.C.; Sharma, Y.C. Adsorption characteristics of alumina nanoparticles for the removal of hazardous dye, Orange G from aqueous solutions. *Arab. J. Chem.* **2019**, *12*, 5339–5354. [CrossRef]
32. Zhou, S.; Antonietti, M.; Niederberger, M. Low-temperature synthesis of y-alumina nanocrystals from aluminum acetylacetonate in nonaqueous media. *Small* **2007**, *3*, 763–767. [CrossRef]
33. Alnajjar, M.; Hethnawi, A.; Nafie, G.; Hassan, A.; Vitale, G.; Nassar, N.N. Silica-alumina composite as an effective adsorbent for the removal of metformin from water. *J. Environ. Chem. Eng.* **2019**, *7*, 102994. [CrossRef]
34. Sayehi, M.; Tounsi, H.; Garbarino, G.; Riani, P.; Busca, G. Reutilization of silicon- and aluminum- containing wastes in the perspective of the preparation of SiO2-Al2O3 based porous materials for adsorbents and catalysts. *Waste Manag.* **2020**, *103*, 146–158. [CrossRef]
35. Mardkhe, M.K.; Huang, B.; Bartholomew, C.H.; Alam, T.M.; Woodfield, B.F. Synthesis and characterization of silica doped alumina catalyst support with superior thermal stability and unique pore properties. *J. Porous Mater.* **2016**, *23*, 475–487. [CrossRef]